nature cell biology

LETTERS

Correlated three-dimensional light and electron microscopy reveals transformation of mitochondria during apoptosis

Mei G. Sun[1], James Williams[1], Cristina Munoz-Pinedo[2], Guy A. Perkins[3], Joshua M. Brown[3], Mark H. Ellisman[3], Douglas R. Green[2] and Terrence G. Frey[1,4]

In addition to their role in cellular bioenergetics, mitochondria also initiate common forms of programmed cell death (apoptosis) through the release of proteins such as cytochrome *c* from the intermembrane and intracristal spaces[1,2]. The release of these proteins is studied in populations of cells by western blotting mitochondrial and cytoplasmic fractions of cellular extracts, and in single cells by fluorescence microscopy using fluorescent indicators and fusion proteins[3,4]. However, studying the changes in ultrastructure associated with release of proteins requires the higher resolution provided by transmission electron microscopy[5–7]. Here, we have used fluorescence microscopy to characterize the state of apoptosis in HeLa cells treated with etoposide followed by electron microscopy and three-dimensional electron microscope tomography of the identical cells to study the sequence of structural changes. We have identified a remodelling of the inner mitochondrial membrane into many separate vesicular matrix compartments that accompanies release of proteins; however, this remodelling is not required for efficient release of cytochrome *c*. Swelling occurs only late in apoptosis after release of cytochrome *c* and loss of the mitochondrial membrane potential.

Concurrent with the recognition of the importance of mitochondria in apoptosis, has been the application of electron microscope tomography, a form of three-dimensional transmission electron microscopy (TEM), to study mitochondrial ultrastructure leading to a new paradigm of mitochondrial structure. Electron microscope tomography reveals that in normal mitochondria the inner membrane has two topologically distinct components: the inner boundary membrane lies closely apposed to the outer membrane with a small space (the intermembrane space, approximately 8 nm thick) between the two. At various loci, the inner membrane projects into the matrix via tubular structures of uniform diameter called crista junctions, which merge to form lamellar crista compartments enclosing the intracristal space[5–8].

In most cell culture models of apoptosis the relevant mitochondrial events, release of cytochrome *c* and loss of the mitochondrial membrane potential ($\Delta\Psi_m$) occur within minutes, while the onset of these changes occurs asynchronously among a population of cells over periods of several hours[3,4] (Fig. 1). To examine the ultrastructure of mitochondria at defined stages of apoptosis in an asynchronous cell population, correlated light and electron microscopy was performed on cells growing in special petri dishes that contain a glass coverslip with an etched grid. The grid allowed identification of successive stages in the apoptotic programme in HeLa cells permanently transfected with fluorescent cytochrome *c* fusion proteins to monitor cytochrome *c* release, and stained with tetramethylrhodamine ethyl ester (TMRE) to monitor $\Delta\Psi_m$[3,4]. The identical cells were subsequently fixed and embedded for TEM, and their ultrastructure was characterized by both conventional thin-section TEM and by three-dimensional electron microscope tomography of semi-thick sections up to 0.5 μm thickness[7]. This method comprises a form of virtual four-dimensional TEM — three spatial dimensions plus time expressed as the stage of apoptosis.

HeLa cells permanently transfected with a cytochrome *c* fusion protein (relative molecular mass, M_r, of 13,300) containing a short tetracysteine motif (Cyt. *c*-4CYS) that binds the membrane-permeable biarsenical fluorescein derivative FlAsH[3,9] are shown in Fig. 1a–f. The cells were treated with etoposide to induce apoptosis, stained with FlAsH to monitor the distribution of Cyt. *c*-4CYS and with TMRE to reveal mitochondria that maintain $\Delta\Psi_m$. Images recorded at the start of the experiment show the distribution of Cyt. *c*-4CYS, mitochondria maintaining a $\Delta\Psi_m$ and an overlay demonstrates localization of Cyt. *c*-4CYS within mitochondria (Fig. 1a–c). Images of the same field of cells 16 h after addition of etoposide reveal two cells (outlined

[1]Department of Biology, San Diego State University, San Diego, CA 92182-4614, USA. [2]Department of Immunology, St Jude Children's Research Hospital, Memphis, TN 38105–2794, USA. [3]Center for Research in Biological Systems, National Center for Microscopy and Imaging Research, University of California, San Diego, La Jolla, CA 92093-0608, USA.
[4]Correspondence should be addressed to T.G.F. (e-mail: tfrey@sunstroke.sdsu.edu)
Received 7 June 2007; accepted 3 August 2007; published online 26 August 2007; DOI: 10.1038/ncb1630

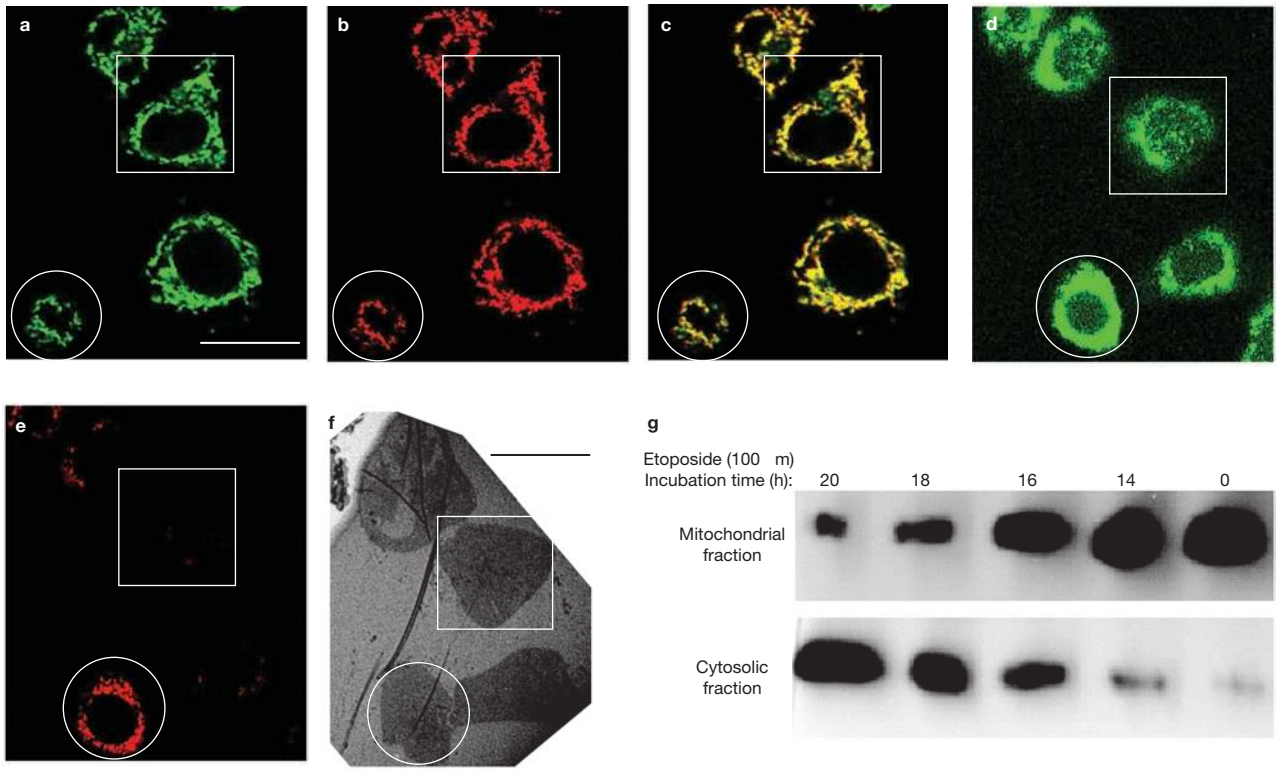

Figure 1 Cyt. *c*-4CYS staining with FlAsH colocalizes with TMRE staining of mitochondria that maintain a $\Delta\Psi_m$. Cyt. *c*-4CYS is released before loss of $\Delta\Psi_m$. HeLa cells transfected with Cyt. *c*-4CYS were grown in petri dishes with a glass coverslip containing an etched grid and then stained with FlAsH and TMRE. Apoptosis was initiated with 100 μM etoposide. (**a**–**c**) Cyt. *c*-4CYS (green), TMRE (red) and the overlay showing overlap of the two signals (yellow) of a field of cells at the start of the experiment (stage 1). (**d**–**e**) The same field of cells as in **a**–**c** 16 h after addition of etoposide. (**f**) A low magnification electron micrograph of the same field of cells after chemical fixation, dehydration and embedding in plastic at 16 h. The circles enclose a cell whose mitochondria have released Cyt. *c*-4CYS but maintains $\Delta\Psi_m$ after 16 h (stage 2). The square encloses a cell whose mitochondria have both released Cyt. *c*-4CYS and lost $\Delta\Psi_m$ after 16 h (stage 3). The scale bars in **a**–**e** represent 25 μm. (**g**) Western blot of total cytochrome *c* in cytosolic and mitochondrial fractions of a population of HeLa cells after treatment with etoposide. Protein aliquots (13 μg) from cytosolic fractions and mitochondrial fractions were prepared 0, 14, 16, 18 and 20 h after etoposide addition and subjected to SDS–PAGE. The proteins were transferred to PVDF and subjected to immunoblotting with anti-cytochrome *c*, and visualized by chemiluminescent ECL substrate. Uncropped images of the scans are shown in the Supplementary Information, Fig. S4.

by a circle and a square) that represent two successive stages in the apoptotic programme in all Fig. 1 components (Fig. 1d–f). The circled cell has released cytochrome *c*, as indicated by diffuse FlAsH staining in Fig. 1d, while maintaining $\Delta\Psi_m$, as indicated by punctate TMRE staining in Fig. 1e. The cell outlined in the square has also released cytochrome *c*, but all of the mitochondria within this cell have lost their $\Delta\Psi_m$. This same field of cells was chemically fixed, dehydrated and embedded in plastic before cutting sections for examination by TEM, and a thin section of this area is shown at low magnification in Fig. 1f. Cells that lost $\Delta\Psi_m$ but maintained punctate FlAsH–Cyt. c-4CYS staining were not observed, confirming that release of cytochrome *c* precedes loss of $\Delta\Psi_m$, as previously reported[3,4]. Western blot analysis of identically treated cells confirms that, among a population of cells, release of native cytochrome *c* is 50% complete within 16–18 h and nearly complete for all cells by 20 h after treatment with etoposide (Fig. 1g).

Based on the changes in fluorescence observed in HeLa cells expressing Cyt. *c*-4CYS labelled with FlAsH and TMRE, three stages during apoptosis initiated by etoposide were identified: stage 1, before release of cytochrome *c* and before loss of $\Delta\Psi_m$; stage 2, after release of cytochrome *c* but before loss of $\Delta\Psi_m$; stage 3, after both release of cytochrome *c* and loss of $\Delta\Psi_m$. Fig. 2 shows fluorescent light and transmission electron micrographs of three different fields of cells at each of the three stages of the apoptotic programme. A field of cells before release of cytochrome *c* and before loss of $\Delta\Psi_m$, as indicated by the punctate FlAsH and TMRE staining that match in the overlay, are observed in stage 1 (Fig. 2a). The higher magnification electron micrograph reveals a number of mitochondria that all have the morphology of the normal orthodox conformation observed in healthy cells. In stage 2, the FlAsH staining is diffuse, indicating that cytochrome *c* has been or is being released, wheras the TMRE staining remains punctate, indicating the presence of $\Delta\Psi_m$ (Fig. 2b). The higher magnification electron micrograph shows many normal mitochondria, but also several mitochondria with an altered morphology that we refer to as 'vesicular' based on electron microscope tomography described below. In stage 3, fluorescence microscopy again reveals the diffuse FlAsH staining indicative of cytochrome *c* release and the now nearly complete absence of TMRE staining, indicating that all of the mitochondria have lost $\Delta\Psi_m$ (Fig. 2c). The higher magnification electron micrograph

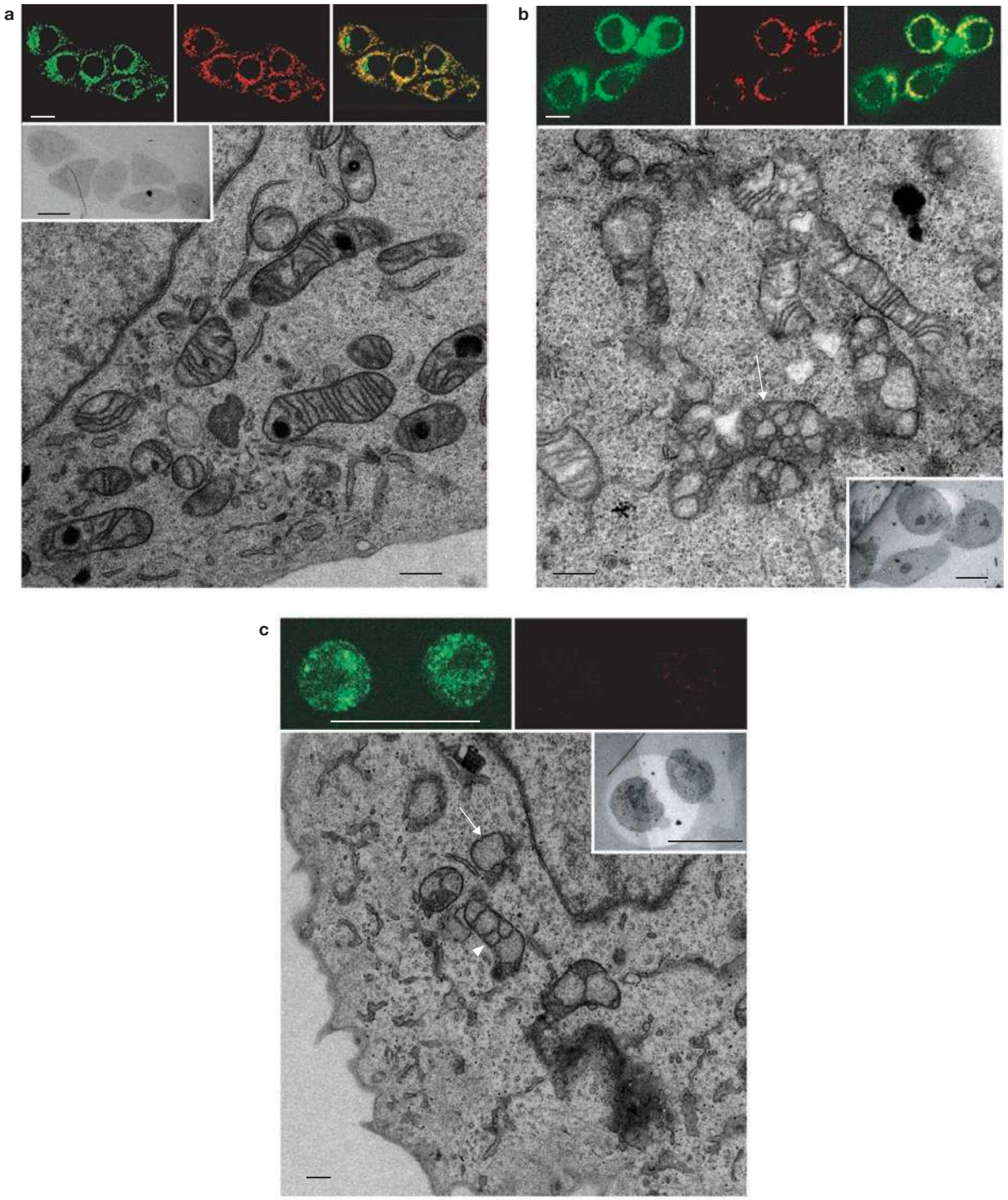

Figure 2 Mitochondrial inner membrane conformation changes to the vesicular form during cytochrome *c* release, and the matrix swells during or after the loss of $\Delta\Psi_m$. HeLa cells transfected with Cyt. *c*-4CYS and stained with FlAsH and TMRE were monitored by confocal microscopy before preparation for electron microscopy of the same fields of cells. (**a**) Stage 1 cells have neither released Cyt. *c*-4CYS nor lost $\Delta\Psi_m$, as indicated by the colocalization of FlAsH staining of Cyt. *c*-4CYS (green) with TMRE staining (red) in the overlay image (yellow). The electron micrographs show only the normal mitochondrial morphology. The inset on the upper left is a low magnification electron micrograph of the complete field of six cells. (**b**) Stage 2 cells have released (or are releasing) Cyt. *c*-4CYS but maintain $\Delta\Psi_m$, as indicated by the diffuse FlAsH staining in the upper left panel that does not correlate with the punctate TMRE staining in the overlay. These cells display both normal mitochondrial morphologies in electron micrographs but also many mitochondria with vesicular matrix compartments with one indicated by the arrow. The inset on the lower right shows a low magnification electron micrograph of this field of four cells. (**c**) Stage 3 cells that have released Cyt. *c*-4CYS and have lost $\Delta\Psi_m$ contain relatively few mitochondria with normal morphology and many with swollen morphology (arrow) and vesicular–swollen mitochondria (arrowhead). The scale bars represent 25 μm in the fluorescent micrographs and low magnification TEMs and 500 nm in the high magnification TEMs.

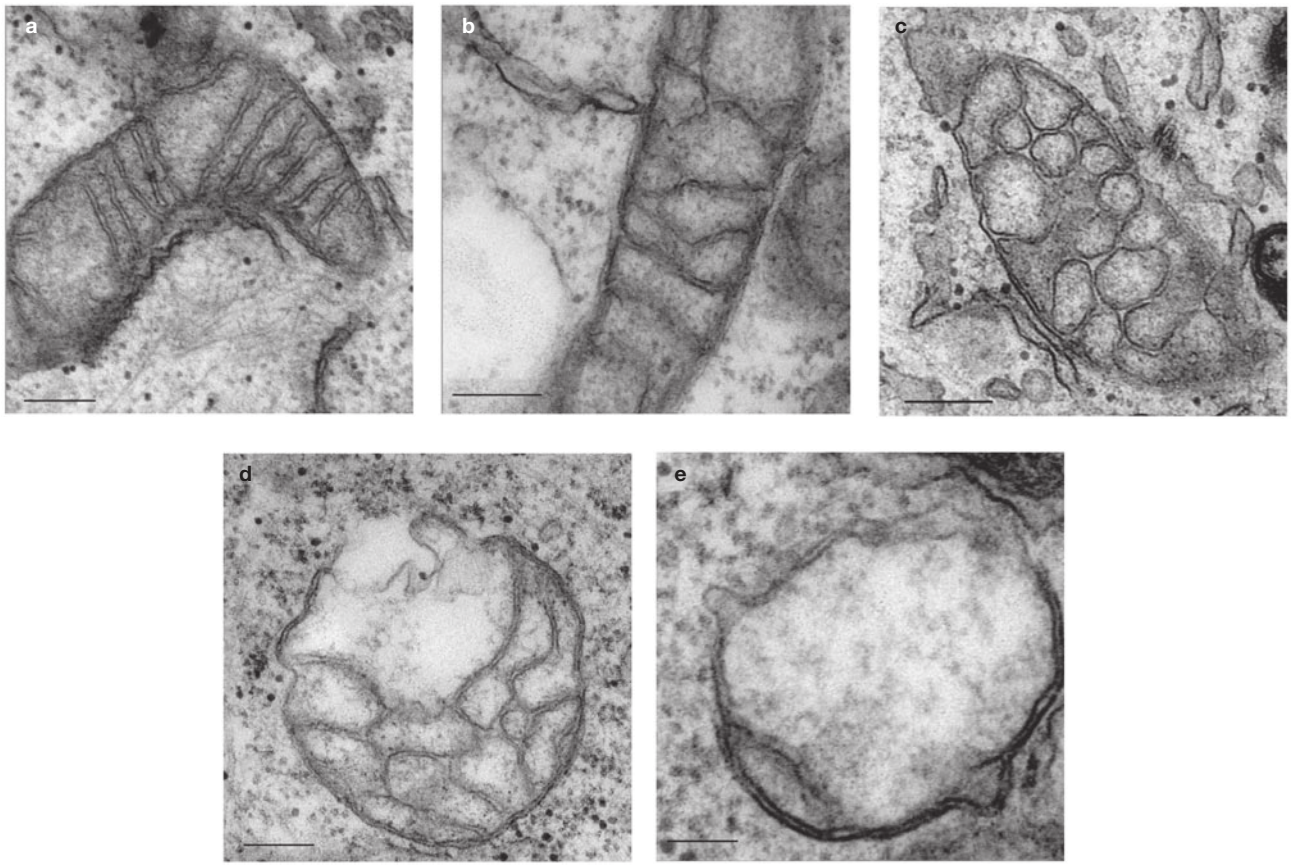

Figure 3 Five mitochondrial morphologies are identified. (**a**) normal; (**b**) normal–vesicular; (**c**) vesicular; (**d**) vesicular–swollen; and (**e**) swollen. The scale bars represent 200 nm in **a**–**d** and 100 nm in **e**.

reveals no normal mitochondria, but does include several mitochondria that appear to be swollen, and some of these also display vesicular morphology.

We have identified five characteristic mitochondrial morphologies based on observation of electron micrographs of cells within the three stages as shown in Fig. 3: normal, Fig. 3a; normal–vesicular, Fig. 3b; vesicular, Fig. 3c; vesicular–swollen, Fig. 3d; and swollen, Fig. 3e. Mitochondria exhibiting the vesicular ultrastructure are easily identified in electron micrographs of thin sections, but characterizing their structure required the third spatial dimension provided by electron microscope tomography (Fig. 4). Electron microscope tomography indicates that in vesicular mitochondria, the inner membrane encloses separate vesicular matrix compartments, the lumen of which is topologically equivalent to the mitochondrial matrix (Fig. 4c and see Supplementary Information, Movie 1). Furthermore, the change in morphology from normal to vesicular is progressive from one region of an extended mitochondrion to another, because intermediate forms designated normal–vesicular display normal cristae within an inner boundary membrane at one end and vesicular matrix compartments at the other (Fig. 4b and see Supplementary Information, Movie 2).

Swollen mitochondria are identified by their expanded matrix space, fewer cristae and less dense staining of the matrix (examples are shown in Figs 2c, 3e and 4e, and see Supplementary Information, Movie 3; note that in the latter, the outer membrane seems to be ruptured by the expanded matrix). Again an intermediate form, vesicular–swollen, is observed in which one domain of a mitochondrion seems swollen, while another domain seems vesicular (Figs 2c, 3d and 4d, and see Supplementary Information, Movie 4).

These unusual mitochondrial inner membrane structures are unlikely to be the result of artifacts of either the specimen preparation procedure or illumination of cells containing multiple fluorophores. As controls, non-transfected HeLa cells, in the absence of fluorophores, were prepared by cryofixation at high pressure followed by freeze substitution — a procedure believed to provide superior structural preservation when properly applied[7]. Vesicular mitochondria were only observed when cells were treated with etoposide for many hours (see Supplementary Information, Fig. S1). Extensively illuminated HeLa cells stained with both FlAsH and TMRE were also observed in the absence of etoposide and no vesicular mitochondria were ever seen in these cells.

To determine the sequence of ultrastructure changes during apoptosis, we recorded numerous electron micrographs of cells in each of the three stages, as determined by fluorescence confocal microscopy, and scored the numbers of mitochondrial profiles with each of the five morphologies. The results are shown in Fig. 5, together with the number of cells and total number of mitochondria measured in each case. As expected, control cells that were not treated with etoposide are defined as stage 1 and displayed only normal

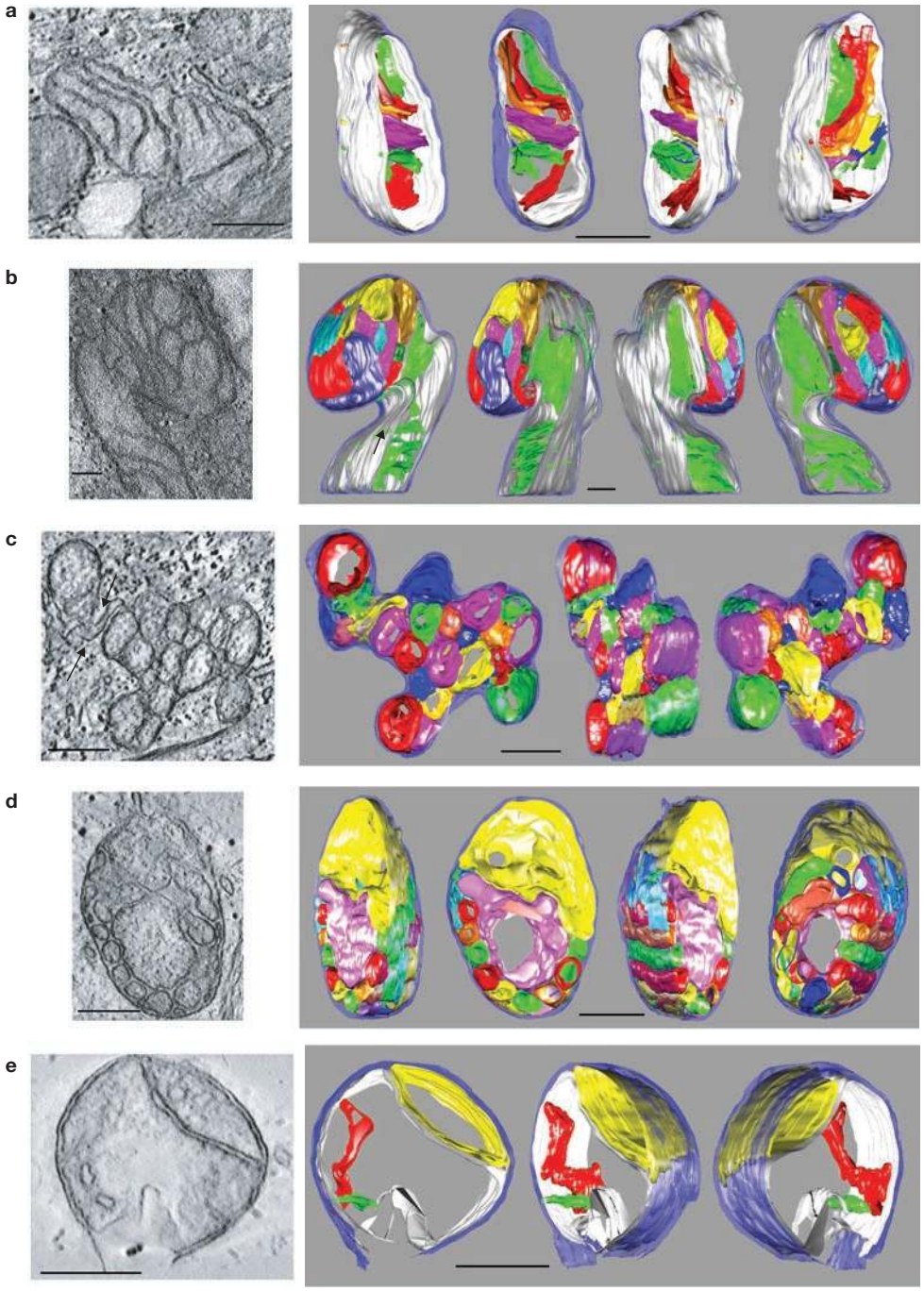

Figure 4 Electron microscope tomography of examples of the five mitochondrial morphologies. On the left are sections of constant *z* through the electron tomograms, and on the right are renderings of the models produced from segmented tomograms. Outer membrane (translucent light blue); the inner boundary membrane (white); cristae in various colours. The successive views rotate about a vertical axis by varying amounts from left to right. (**a**) Normal mitochondrion with the outer membrane in the leftmost and two rightmost views reduced to reveal the small discrete crista junctions (red, green, and yellow; see Supplementary Information, Movie 7). (**b**) Normal–vesicular mitochondrion with the vesicular portion at the top and different vesicular matrix compartments indicated in various colours. The normal portion is below and the normal cristae (green) are contained within the matrix compartment enclosed within the inner boundary membrane (white). The arrow indicates an elongated crista junction (see Supplementary Information, Movie 2). (**c**) Vesicular mitochondrion with the vesicular matrix compartments containing the fragmented matrix in various colours; note, there is no inner boundary membrane (see Supplementary Information, Movie 1). (**d**) Vesicular–swollen mitochondrion with two swollen vesicular matrix compartments indicated in yellow (upper end) and in magenta (centre), and small vesicular matrix compartments (in various colours) surrounding the magenta swollen vesicular compartment; note again, the absence of an inner boundary membrane (see Supplementary Information, Movie 4). (**e**) Swollen mitochondrion with one swollen vesicular matrix compartment (yellow) and two lamellar cristae (red and green) contained within a swollen matrix bound by an inner boundary membrane (white); note that the outer membrane seems to be ruptured at the bottom (see Supplementary Information, Movie 3). The scale bars represent 250 nm.

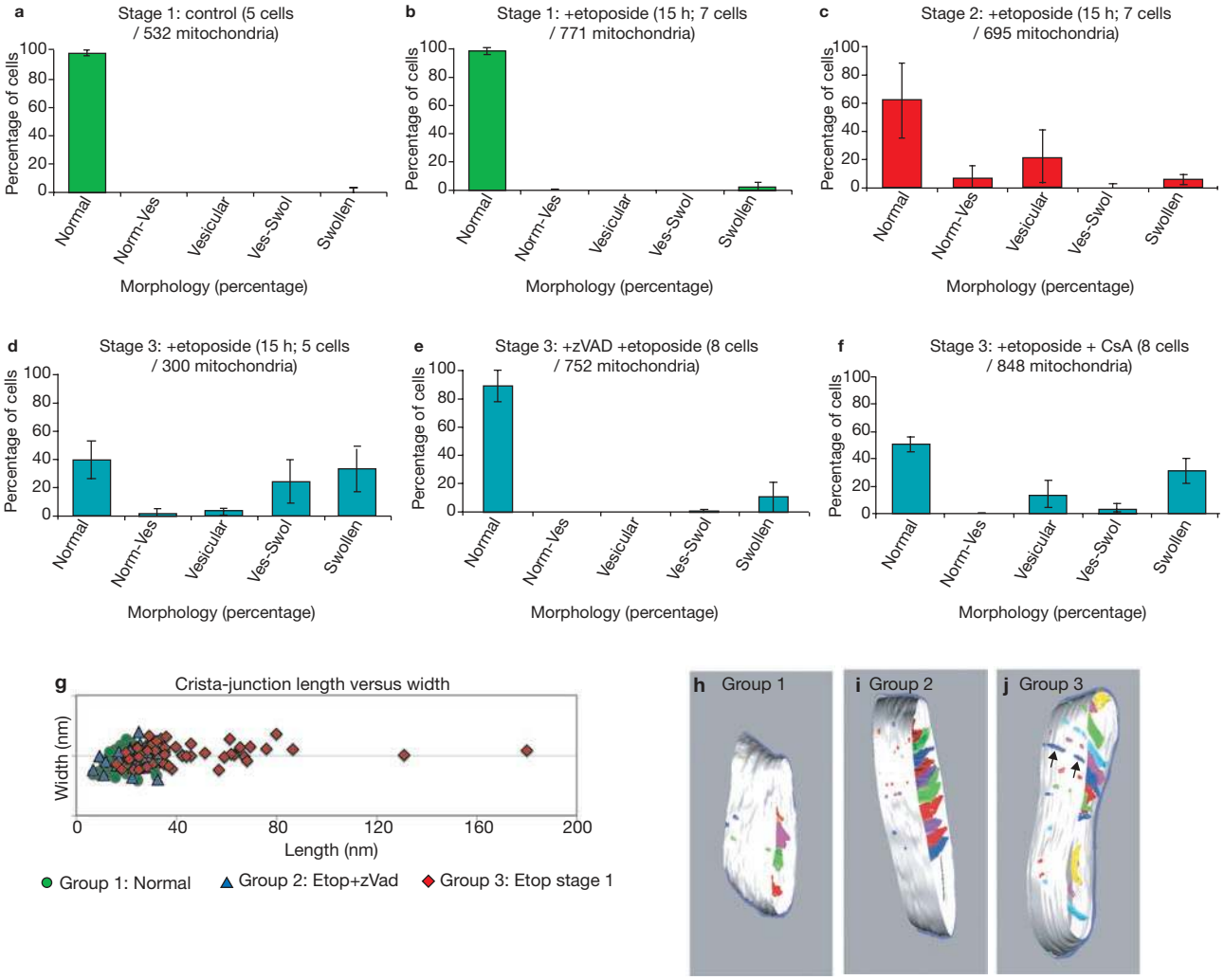

Figure 5 Mitochondria progress from normal to vesicular during release of cytochrome *c* and then swell during or after the loss of $\Delta\Psi_m$. (**a**–**f**) Histograms showing the percentage of mitochondria observed within each of the five morphologies for cells in stages 1–3. Cells were selected based on FlAsH and TMRE staining of HeLa cells transfected with Cyt. *c*-4CYS (see Fig. 2 for examples). Electron micrographs of each cell were collected and all of the mitochondria within a thin section of each cell were classified in a double-blind fashion. The number of cells and total number of mitochondria analysed are indicated at the top of each graph. The error bars represent the s.d. of the percentage of mitochondria with each morphology within the group of cells analysed for each stage, and show greater variation for stages 2 and 3 as cells in these categories represent times along a continuum of structural change. Stage 1, control cells with no treatment (**a**). Stage 1, treatment with etoposide for 15 h; Cells have not released Cyt. *c*-4CYS and maintain $\Delta\Psi_m$ (**b**). Stage 2, treatment with etoposide for 16 h; cells have released Cyt. *c*-4CYS but maintain $\Delta\Psi_m$ (**c**). Stage 3, treatment with etoposide for 16 h; cells have released Cyt. *c*-4CYS and have lost $\Delta\Psi_m$ (**d**). Stage 3 with caspases inhibited and treatment with etoposide for 16 h in the presence of zVAD-fmk; cells have released Cyt. *c*-4CYS and have lost $\Delta\Psi_m$ (**e**). Stage 3 with mPTP inhibited and treatment with etoposide for 16 h in the presence of cyclosporin A; cells have released Cyt. *c*-4CYS and have lost $\Delta\Psi_m$ (**f**). (**g**) z-VAD-fmk inhibits crista junction elongation. The length (the longest dimension) and width (the shortest dimension orthogonal to the length) of 50 crista junctions from each of three groups of HeLa cells were measured by Image J from the tomograms. Group 1, untreated control (measured from five tomograms); Group 2, stage 3 HeLa cells pretreated with zVAD to inhibit caspases and treated with etoposide for 16 h (measured from three tomograms); Group 3, stage 1 are cells treated with etoposide for 15 h (measured from four tomograms). (**h**–**j**) Three-dimensional models from electron microscope tomography of mitochondria representing each of the three groups described in **g**. Arrows in the group 3 tomogram indicate elongated crista junctions.

mitochondrial profiles with a very low number of swollen mitochondria. Cells treated with etoposide for 15 h and imaged before either the release of cytochrome *c* or loss of $\Delta\Psi_m$ were also defined as stage 1, and they contained only normal mitochondrial profiles (Fig. 5b). Stage 2 mitochondria had released cytochrome *c* but maintained a normal $\Delta\Psi_m$, and although a small majority (62%) of mitochondria still displayed a normal profile, there was a significant number that exhibited vesicular morphology, with a total of 32% falling into the normal–vesicular, vesicular or vesicular–swollen morphologies, and approximately 6% in the swollen category. Stage 3 mitochondria had released cytochrome *c*, lost $\Delta\Psi_m$ and exhibited a further shift away from the normal structure (down to 39%) toward

the vesicular and swollen structures (Fig. 5d). We interpreted this to indicate that the progression of change is from the normal structure to the vesicular during or immediately after cytochrome *c* release, then progressing to a swollen morphology after the loss of $\Delta\Psi_m$. This progression of change is indicated by the greater variation of the distributions of morphologies among the individual cells in stages 2 and 3, as each cell seemingly represents a different point along a continuum of changes grouped within each classification or stage. Note that even stage 3 cells still contain 39% normal mitochondria, and we do not know whether all mitochondrial cristae convert to vesicular morphology before swelling.

To evaluate the importance of caspase activation, the experiment was repeated in the presence of the general caspase inhibitor, zVAD-fmk, which inhibited caspases by more than 54% (data not shown). Caspase-inhibited cells in stage 3 maintained normal mitochondrial structure (89%), with a small number of swollen mitochondria (11%, Fig. 5e). Thus, transformation to the vesicular structure seems to require active caspases. We also examined the possible participation of the mitochondrial permeability transition pore (mPTP) by conducting the experiment in the presence of cycloporin-A (CsA). As expected CsA treatment inhibited opening of the mPTP, as it prevented the release of calcein trapped within mitochondria (see Supplementary Information, Fig. S2)[10], but it did not inhibit cytochrome *c* release or prevent the transformation to the vesicular structure (Fig. 5f).

We wanted to determine whether mitochondrial swelling and/or inner mitochondrial membrane remodelling occured during apoptosis, and whether either swelling or inner membrane remodelling was required for release of cytochrome *c*. The answers are yes and no, respectively. Significant swelling occurs only after loss of $\Delta\Psi_m$ and long after release of cytochrome *c* (Fig. 5). Although formation of vesicular mitochondria is observed during release of cytochrome *c*, and would facilitate diffusion of cytochrome *c* from intracristal compartments, vesicular mitochondria comprise a minority of mitochondrial structures until after the loss of $\Delta\Psi_m$. More significantly, inhibition of caspases by addition of zVAD-fmk completely prevents the transformation to vesicular mitochondria. A more subtle question is whether crista-junction size must increase to facilitate release of cytochrome *c* from the intracristal spaces as previous observations indicate that cytochrome *c* release accompanies an enlargement and elongation of crista junctions following treatment of purified rodent liver mitochondria with truncated Bid[11,12]. Crista-junction sizes were measured in mitochondria in untreated cells, in mitochondria in stage 3 cells treated with etoposide in the presence of zVAD-fmk and in stage 1 etoposide-treated cells (Fig. 5g–j). Normal mitochondria, and mitochondria in cells treated with etoposide in the presence of zVAD-fmk, displayed overlapping distributions of crista-junctions sizes with relatively isotropic diameters centred at approximately 20 nm, and the stage 3 cells treated with etoposide in the presence of zVAD-fmk released cytochrome *c* and lost $\Delta\Psi_m$. Although the 20 nm crista-junction diameter is several times the diameter of cytochrome *c*, the junctions could present a kinetic barrier to efficient release of cytochrome *c*. However, kinetic modelling studies indicate that crista junctions should not prevent release of intracristal cytochrome *c* within 1–2 min[13]. Furthermore, it was previously shown that although the cytochrome *c* in the intermembrane space and the intracristal space represented separate pools on a fast time scale, essentially all cytochrome *c* within purified mitochondria is reduced by externally added NADH via NADH-cytochrome b_5 reductase in the outer mitochondrial membrane within 1–2 min[14] — approximately the time measured for release of cytochrome *c* from mitochondria during apoptosis[3,4].

The vesicular mitochondrial phenotype has been observed under other conditions, and even in intact tissues, establishing that it is not merely a curiosity confined to our particular cultured-cell model. OPA1 (mgm1p in yeast) is a dynamin-related protein found in the mitochondrial intermembrane space, and is believed to function in determining inner mitochondrial membrane conformation and crista-junction shape and size, as well as mediate inner membrane fusion[11,15–17]. During suppression of *OPA1* expression with short interfering RNA (siRNA) to model the most common form of autosomal dominant optic atrophy (ADOA), mitochondrial structures that seem identical to those that we have identified as vesicular were observed[18]. More significantly, mitochondria with a morphology identical in thin sections to our vesicular mitochondria were observed in muscle tissue from mice deficient in collagen VI created as a model for Bethlehem myopathy, a heritable human muscle disease[19].

If not required for efficient release of cytochrome *c* the vesicular transformation of the mitochondrial inner membrane may have another function or relevance: a possibility is in the fragmentation of the mitochondrial network that accompanies apoptosis[20–23]. Vesicular mitochondria contain fragmented vesicular-matrix compartments, and subsequent fragmentation of the mitochondrial network requires only outer membrane fission. In this context, it is interesting to note that mitochondria in stage 1 etoposide-treated cells displayed many crista junctions with an elongated shape: these mitochondria had one short dimension, plotted as the 'width' in Fig. 5g, whose distribution matches the more isotropic diameters of crista junctions in normal mitochondria. The elongated crista junctions exhibited a much greater length of up to 180 nm (Fig. 5j and see Supplementary Information, Movie 5). This observation suggests a facile mechanism for the transformation of normal mitochondria into the vesicular form by elongation and fusion of crista junctions around the perimeter of lamellar cristae, as shown in the Supplementary Information, Fig. S3 and Movie 6. This achieves fragmentation of the matrix into separate vesicular matrix compartments without compromising the integrity of the matrix. The fact that suppression of *OPA1* expression by siRNA produces a similar phenotype[18] suggests that the inner-membrane transformation to vesicular-matrix compartments may represent the mechanism for inner-membrane fission that occurs throughout the mitochondria in the formation of vesicular mitochondria, but would normally occur only at the sites of outer-membrane fission during the normal mitochondrial-fission process.

Although these results indicate that mitochondrial swelling is an effect, rather than a proximate cause, of apoptosis initiated in the mitochondrial pathway, it is important to keep in mind that under other conditions apoptosis may proceed by a different mechanism[1]. We have recently shown that, in HeLa cells, initiation of apoptosis by addition of H_2O_2 results in immediate loss of $\Delta\Psi_m$, subsequent activation of the mPTP and large amplitude swelling of the mitochondrial matrix, which seems, in this case, to be the immediate cause of cytochrome *c* release (M.G.S., unpublished observations). □

METHODS

Culture conditions and the induction of apoptosis. HeLa cells expressing Cyt. *c*-4CYS were previously described[3] and were grown and maintained at 37 °C in DMEM (Gibco, Carlsbad, CA) supplemented with 10% FBS, 2 mM L-glutamine, 200 mg ml^{-1} penicillin and 100 mg ml^{-1} streptomycin sulphate in a humidified atmosphere of 5% CO_2:95% air. Cells were subcultured 1:10 by incubating them in 0.25% trypsin (Gibco) when they were confluent and resuspending cells in growth medium.

Apoptosis was induced with 100 μM etoposide for 12–18 h. Where indicated, zVAD-fmk (100 μM; Sigma, St Louis, MO) was added 12 h before the apoptotic stimulus to inhibit caspase activity. TMRE (50 nM; Sigma) was added to monitor the $\Delta\Psi_m$ and, where indicated, cyclosporin A (CsA, 0.1 μM; Sigma) was used to inhibit opening of the mitochondrial transition pore (mPTP).

Cytochrome *c* labelling with biarsenical ligands. The staining media were prepared by the addition of a premixed DMSO stock solution to give a final concentration of 2.5 μM of FlAsH-1,2-ethanedithiol $(EDT)_2$ and 10 μM EDT (Fluka, St Louis, MO) in DMEM. Cells were incubated at 37 °C in an incubator for 1 h, rinsed in glucose-containing Hanks' buffered saline solution (HBSS; Gibco) and incubated for 10 min at room temperature in HBSS containing 62.5 μM EDT. Cells were washed three times with HBSS and returned to the incubator for at least 12 h before treatment.

Western blotting to detect cytochrome *c* release from HeLa cells. HeLa cells were incubated with etoposide (100 μM) and collected at 0 h, 14 h, 16 h, 18 h and 20 h. Cells were then treated with lysis buffer (80 mM KCl, 250 mM sucrose, 500 μg ml^{-1} digitionin, 0.1 mM PMSF, 1 mM DTT, 1:800 protease inhibitors) for 5 min and centrifuged for 5 min at 10,000*g* at 4 °C. The supernatant (cytosolic fractions) and pellets (mitochondrial fractions) were used for western blot analysis of 13 μg of total protein aliquots subjected to SDS–PAGE. The proteins were transferred to PVDF membranes and subjected to immunoblotting with anti-cytochrome *c* (BD Biosciences, San Jose, CA). Film was developed after incubation of the PVDF with SuperSignal West Pico Chemiluminescent ECL Substrate (Pierce, Rockford, IL).

Calcein-AM to monitor mPTP. HeLa cells were incubated with calcein-AM (2 μM; Invitrogen, Carlsbad, CA) and $CoCl_2$ (1 mM) for 60 min at 37 °C. The cytosolic and nuclear calcein signal is quenched by $CoCl_2$, and mPTP opening was detected by a rapid release of mitochondrial calcein fluorescence.

Confocal microscopy. For time-lapse analysis, cells were grown in 35 mm microwell dishes containing a glass coverslip with an etched grid (MatTek Corp., Ashland, MA). Images were acquired using a Leica TCS SP2 inverted confocal microscope. Cyt.*c*-4CYS–FlAsH, and calcein were excited using the 488 nm line from an Ar–Kr laser attenuated to 35%. TMRE was excited using a 543 nm line from an Ar–Kr laser attenuated to 34%. The detector slits of the confocal microscope were adjusted to detect FlAsH emission between 497–553 nm, TMRE emission between 555–620 nm and calcein emission between 497–553 nm.

Single-cell analysis of mitochondrial structure by correlated confocal and electron microscopy/tomography. After confocal imaging, cells were fixed immediately by a 1 h incubation on ice in a 2.5% paraformaldehyde, 2.5% glutaraldehyde, 0.1 M sodium cacodylate pH 7.4 buffer. After washing three times in ice-cold 0.1 M sodium cacodylate buffer containing 3 μM calcium chloride for 3 min, the primary fixed cells were then incubated with 1% osmium tetroxide, 0.8% potassium ferrocyanide, 3 μM calcium chloride in 0.1 M sodium cacodylate for 60 min on ice. After washing with distilled water three times for 3 min, fixed cells were stained and stabilized in ice-cold 2% uranyl acetate for 30 min on ice and dehydrated in an ice-cold ethanol series of 20%, 50%, 70% and 90% successively on ice for 3 min each. The cells were then dehydrated at room temperature three times for 3 min each in 100% ethanol and infiltrated in well-mixed 50% ethanol, 50% Durcupan ACM resin (Fluka) for 60 min with agitation at room temperature followed by 100% Durcupan ACM twice for 1 h with agitation, after which the samples were placed in an oven and allowed to polymerize at 60–80 °C for at least 48 h. The glass coverslip was peeled away from the bottom using a razor blade and the selected area was cut out and glued to a block for sectioning. Thin sections (approximately 80 nm) were collected and pre-stained with 2% uranyl acetate and Sato lead before examination in an FEI Tecnai 12 TEM.

For electron microscope tomography, single-tilt series three-dimensional reconstructions were obtained from semi-thick samples (250–500 nm) in a tilt-series every 2° from –60° to +60° on a JOEL 4000EX electron microscope operated at 400 kV. The IMOD software suite was used to process the images in each tilt series (Boulder Laboratory for three-dimensional electron microscopy of cells, University of Colorado, Boulder, CO). X-Voxtrace software enabled volume segmentation of tomographic data using manual tracing followed by rendering using Synu (National Center for Microscopy and Imaging Resources, University of California, San Diego, CA). Tomograms were converted to Tiff stacks for measurements of crista junction sizes using Image J (http://rsb.info.nih.gov/ij/).

High-pressure freezing. HeLa-cell pellets were loaded into the 100 μm-deep well of a type A brass planchettes (Ted Pella, Inc., Redding, CA) and covered with the flat side of brass type B planchettes. The planchette A and B sandwiches were quickly loaded into the freezing holder and frozen in a Bal-Tec HPF 010 high pressure-freezing machine. The sandwich was separated under liquid nitrogen and the type A planchette that held the cells was placed in a cryo-vial filled with 2% osmium and 0.1% uranyl acetate in acetone (electron microscopy grade; Fullam Inc., Latham, NY). Freeze substitution was carried out in a Leica EM AFS raising the temperature to –90 °C over 72 h, then to 0 °C over 2 h, and finally to room temperature over 4 h. After substitution, the specimens were rinsed in pure acetone three times (10 min at room temperature). The specimens were removed from planchettes after the last wash and infiltrated with 30% Durcupan in acetone for 2 h, 50% Durcupan overnight, 70% Durcupan for 4 h, 90% over 2 h and 100% Durcupan overnight. The next day, the 100% Durcupan was changed twice more and the resin polymerized in the oven at 60 °C overnight.

Caspase-3 assay. Caspase-3 activity was measured using a caspase-3 fluorogenic substrate, Ac-DEVD-AFC (Sigma). Cells were lysed on ice by lysis buffer (0.71% NP-40, 71 mM Tris t pH 7.5, 0.71 mM EDTA, 212 mM NaCl). The protein concentration of the resulting supernatant was determined using the Bio-Rad DC protein assay. Equal amounts of total cell lysate protein (40 μg) were mixed with caspase-3 assay buffer (21 mM HEPES, 105 mM NaCl, 5.35 mM DTT) containing substrate Ac-DEVD-AFC (25 μM) in a black 96-well titre plate, in triplicate. Caspase-3 mediated cleavage of Ac-DEVD-AFC into free AFC was measured using a Spectra Max Gemini XS flourimeter plate reader with an excitation wavelength of 400 nm and emission wavelength of 505 nm using Softmax Pro version 3.1.2 software replicated three times.

Note: Supplementary Information is available on the Nature Cell Biology website.

ACKNOWLEDGEMENTS

This project was supported by a Blasker Science and Technology Grant from the San Diego Foundation to T.G.F., by the National Institutes of Health (NIH) National Center for Research Resources (Grant No. P41 RR004050; G.A.P. and M.H.E.), by NIH Roadmap Grant GM72033 (Roger Y. Tsien and M.H.E.) and by NIH Grants AI40646, AI52735 and CA69381 (D.R.G.). C.M.-P. was supported by the Secretaria de Estado de Universidades Investigacion and the Fondo de Investigaciones Sanitarias of Spain. We thank Y. Jones (National Center for Microscopy and Imaging Research, University of California, San Diego) for assistance with high pressure freezing and freeze substitution, and J. Nulton for suggesting the mechanism of transformation mitochondria to the vesicular form.

COMPETING FINANCIAL INTERESTS

The authors declare no competing financial interests.

Published online at http://www.nature.com/naturecellbiology/
Reprints and permissions information is available online at http://npg.nature.com/reprintsandpermissions/

1. Green, D. R. & Kroemer, G. The pathophysiology of mitochondrial cell death. *Science* **305,** 626–629 (2004).
2. Shiozaki, E. N. & Shi, Y. Caspases, IAPs and Smac/DIABLO: mechanisms from structural biology. *Trends Biochem. Sci.* **29,** 486–494 (2004).
3. Goldstein, J. C. *et al.* Cytochrome *c* is released in a single step during apoptosis. *Cell Death Differ.* **12,** 453–462 (2005).
4. Goldstein, J. C., Waterhouse, N. J., Juin, P., Evan, G. I. & Green, D. R. The coordinate release of cytochrome *c* during apoptosis is rapid, complete and kinetically invariant. *Nature Cell Biol.* **2,** 156–162 (2000).
5. Frey, T., Renken, C. & Perkins, G. Insight into mitochondrial structure and function from electron tomography. *Biochim. Biophys. Acta.* **1555,** 196–203 (2002).

6. Frey, T. G. & Mannella, C. A. The internal structure of mitochondria. *Trends Biochem. Sci.* **25,** 319–324 (2000).
7. Frey, T. G., Perkins, G. A. & Ellisman, M. H. Electron tomography of membrane-bound cellular organelles. *Annu. Rev. Biophys. Biomol. Struct.* **35,** 199–224 (2006).
8. Mannella, C. A. The relevance of mitochondrial membrane topology to mitochondrial function. *Biochim. Biophys. Acta.* **1762,** 140–147 (2006).
9. Gaietta, G. *et al.* Multicolor and electron microscopic imaging of connexin trafficking. *Science* **296,** 503–507 (2002).
10. Petronilli, V. *et al.* Transient and long-lasting openings of the mitochondrial permeability transition pore can be monitored directly in intact cells by changes in mitochondrial calcein fluorescence. *Biophys. J.* **76,** 725–734 (1999).
11. Frezza, C. *et al.* OPA1 controls apoptotic cristae remodeling independently from mitochondrial fusion. *Cell* **126,** 177–189 (2006).
12. Scorrano, L. *et al.* A distinct pathway remodels mitochondrial cristae and mobilizes cytochrome *c* during apoptosis. *Dev. Cell* **2,** 55–67 (2002).
13. Manor, J. C. *et al.* in *International Conference on Bioinformatics and Computational Biology* 310–314 (CSREA Press, Las Vegas; 2006).
14. Bernardi, P. & Azzone, G. F. Cytochrome *c* as an electron shuttle between the outer and inner mitochondrial membranes. *J. Biol. Chem.* **256,** 7187–7192 (1981).
15. Cipolat, S. *et al.* Mitochondrial rhomboid PARL regulates cytochrome *c* release during apoptosis via OPA1-dependent cristae remodeling. *Cell* **126,** 163–175 (2006).
16. Meeusen, S. *et al.* Mitochondrial inner-membrane fusion and crista maintenance requires the dynamin-related GTPase Mgm1. *Cell* **127,** 383–395 (2006).
17. Shaw, J. M. & Nunnari, J. Mitochondrial dynamics and division in budding yeast. *Trends Cell Biol.* **12,** 178–184 (2002).
18. Griparic, L., van der Wel, N. N., Orozco, I. J., Peters, P. J. & van der Bliek, A. M. Loss of the intermembrane space protein Mgm1/OPA1 induces swelling and localized constrictions along the lengths of mitochondria. *J. Biol. Chem.* **279,** 18792–18798 (2004).
19. Irwin, W. A. *et al.* Mitochondrial dysfunction and apoptosis in myopathic mice with collagen VI deficiency. *Nature Genet.* **35,** 367–371 (2003).
20. Chan, D. C. Mitochondrial fusion and fission in mammals. *Annu. Rev. Cell Dev. Biol.* **22,** 79–99 (2006).
21. Heath-Engel, H. M. & Shore, G. C. Mitochondrial membrane dynamics, cristae remodelling and apoptosis. *Biochim. Biophys. Acta.* **1763,** 1277–1280 (2006).
22. Karbowski, M. *et al.* Quantitation of mitochondrial dynamics by photolabeling of individual organelles shows that mitochondrial fusion is blocked during the Bax activation phase of apoptosis. *J. Cell Biol.* **164,** 493–499 (2004).
23. Lee, Y. J., Jeong, S. Y., Karbowski, M., Smith, C. L. & Youle, R. J. Roles of the mammalian mitochondrial fission and fusion mediators Fis1, Drp1, and Opa1 in apoptosis. *Mol. Biol. Cell* **15,** 5001–5011 (2004).

nature cell biology

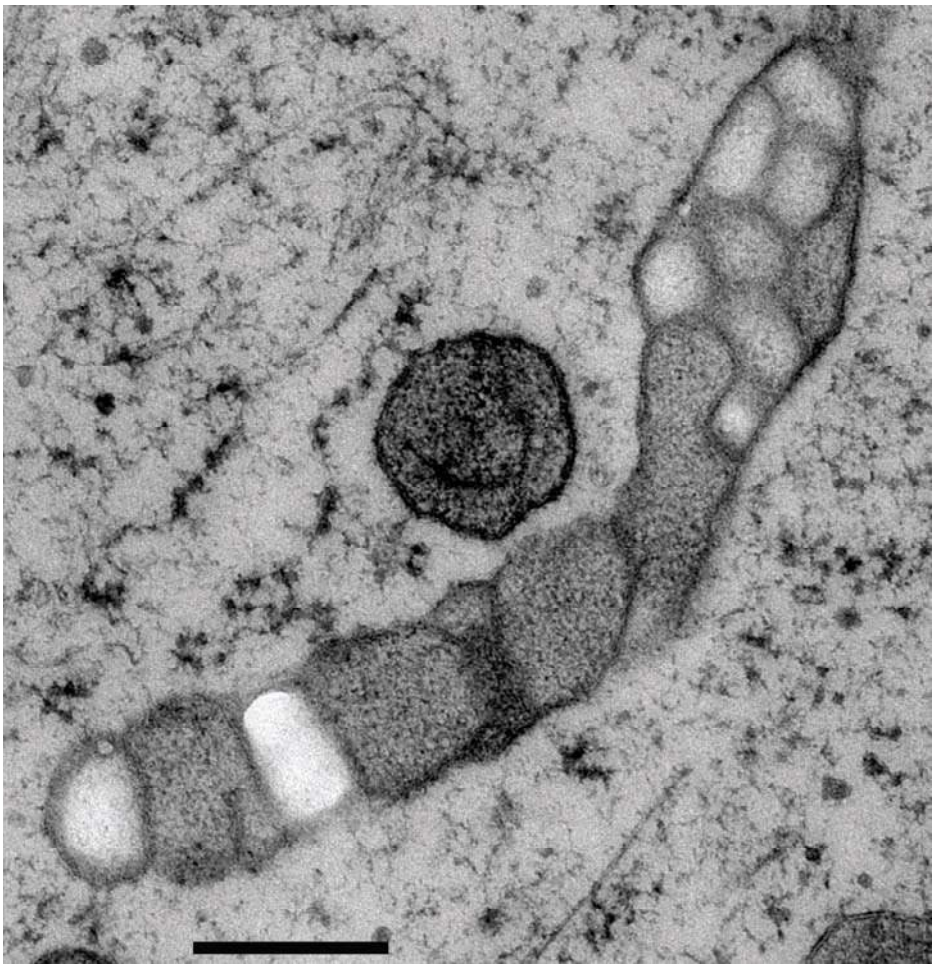

Supplementary Figure 1. High Pressure Freezing Method confirms mitochondrial structure in Etoposide treated HeLa cells.

Wild Type HeLa cells were treated with Etoposide for 16 hours. A pelleted sample was cryofixed by freezing in a Bal-Tec HPF 010 high pressure freezing apparatus followed by freeze substitution and embedding in Durcupan for sectioning. Only cells treated with etoposide showed vesicular mitochondria. Scale bar is 250 nm.

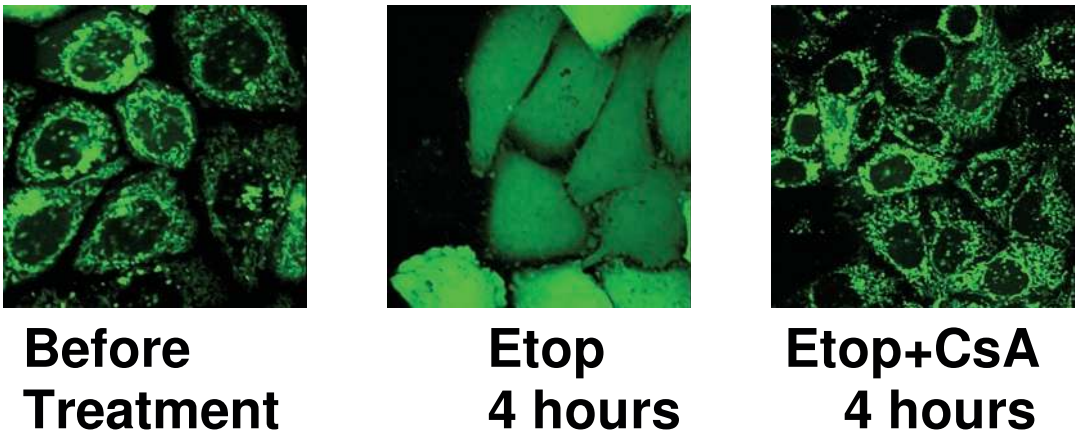

Supplementary Figure 2. Cyclosporin A (CsA, 0.1 M) inhibits mPTP opening:

HeLa cells were treated with etoposide (1mM) for 4 hours. Opening of the mPTP (mitochondria permeability transition pore) was determined by monitoring the release of fluorescent calcein trapped in mitochondria. Confocal images revealed the mPTP opened within 4 hours following treatment with etoposide, while Cyclosporin A inhibited mPTP opening after 4 hours treatment.

Supplementary Figure 3

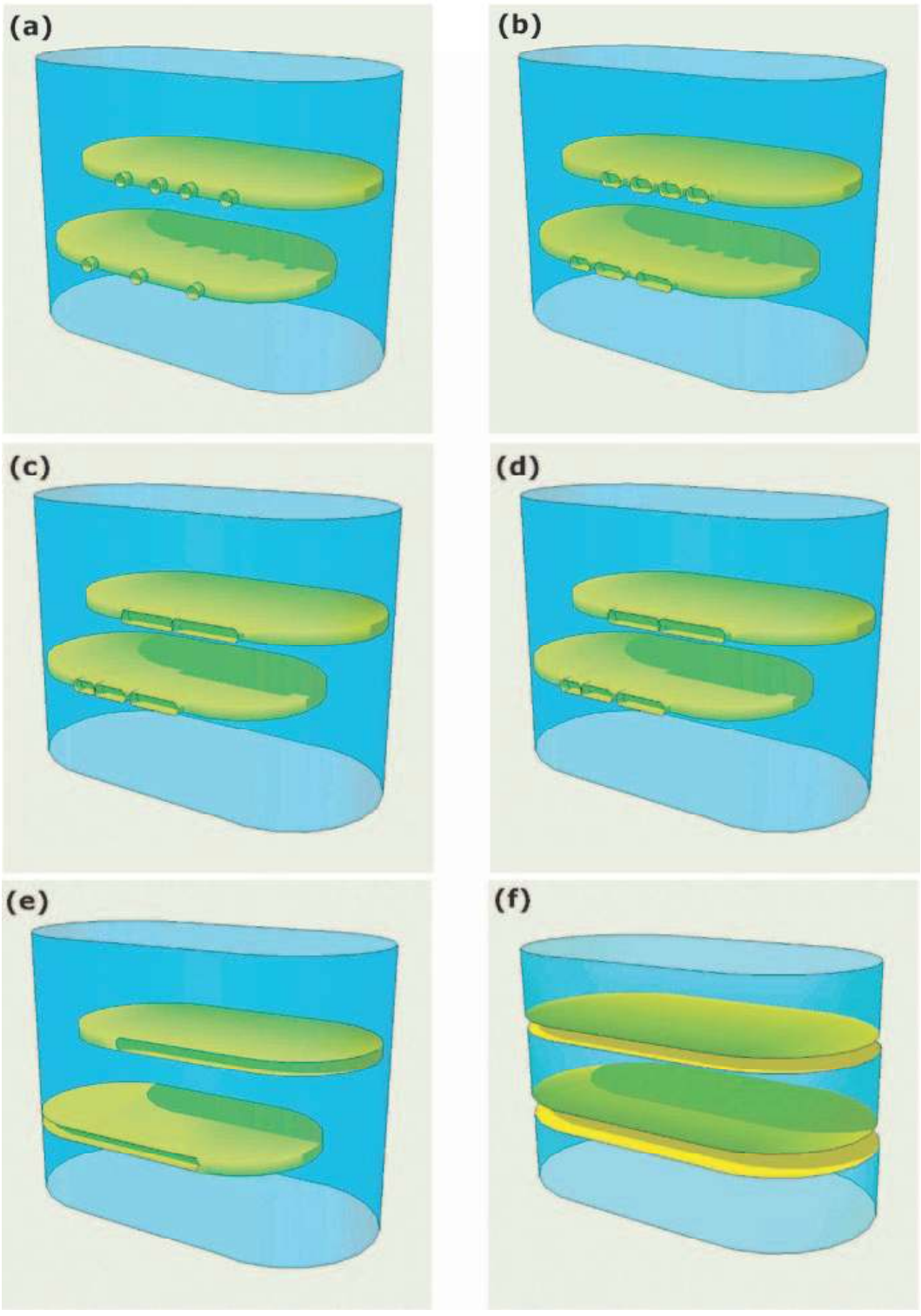

Supplementary Figure 3. A schematic topological model by which normal mitochondria transform to vesicular mitochondria by elongation of crista junctions until nearest neighbors within each lammelar crista fuse followed by continued elongation of the fused crista junctions around the perimeter of the crista.

(a) Schematic model of the inner membrane of a normal orthodox mitochondrion; the outer membrane is not included. The two lamellar cristae in opaque yellow are connected to the inner boundary membrane in translucent blue that surrounds them through short tubular crista junctions, four in the upper crista and three in the lower crista. The cristae plus the inner boundary membrane are one complex two dimensional surface. The ends of the mitochondrion at the top and bottom are not modeled for simplification.

(b - d) The crista junctions in each lamellar crista elongate around the perimeter of the cristae and fuse to form slot like crista junctions.

(e) The crista junctions have elongated completely around the perimeter of what were previously lamellar cristae separating the matrix into three separate vesicular matrix compartments. The model continues to show the distinction between yellow opaque crista membrane and translucent light blue inner boundary membrane with the former crista membranes forming the upper and lower boundaries of the matrix compartments; however, in vesicular mitochondria this distinction is no longer relevant, and the shapes of the vesicular compartments would be round. Three-dimensional models were created with Google SketchUp 5 (www.sketchup.com). See also Movie 6 in Supplementary Information.

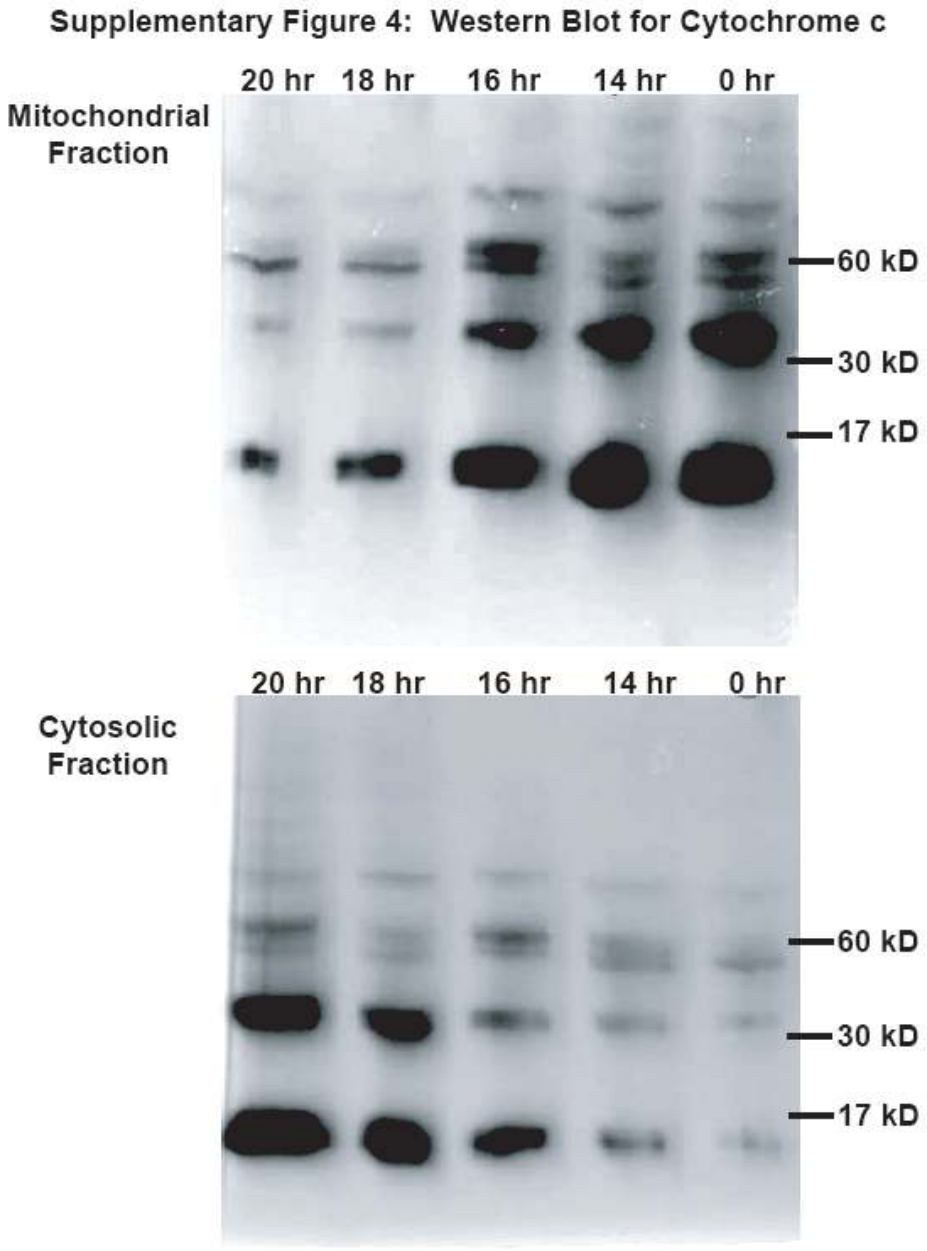

Supplementary Figure 4. Western for cytochrome c of mitochondrial and cytosolic fractions following treatment of HeLa cells with etoposide for 20, 18, 16, 14, and 0 hours respectively. Molecular weight markers are shown on the right. The second band at approximately 30 kD is commonly observed by ourselves and others and its changes follow closely the band at approximately 14 kD; it is probably a cytochrome *c* dimer. Molecular weights are approximate based upon Multi Mark Standards (Invitrogen).

MOVIE LEGENDS

Movie 1: Vesicular Mitochondrion: Model based upon a segmented EM Tomogram of a mitochondrion in a HeLa cell treated with Etoposide for 16 hours. Outer membrane is rendered in translucent blue and surrounds multiple vesicular matrix compartments of various sizes rendered in different colors. No inner boundary membrane is present.

Movie 2: Normal Vesicular Mitochondrion: Model based upon a segmented EM Tomogram of a mitochondrion in a HeLa cell treated with Etoposide for 16 hours. Outer membrane is rendered in translucent blue, note inner boundary membrane at one end of the mitochondrion rendered in opaque white with cristae rendered in green, and crista junctions that have anisotropic dimensions with lengths often greater than widths. The opposite end of the mitochondrion contains vesicular matrix compartments of various sizes rendered in different colors surrounded by outer membrane with no inner boundary membrane.

Movie 3: Swollen Mitochondrion: Model based upon a segmented EM Tomogram of a mitochondrion in a HeLa cell treated with Etoposide for 16 hours. Outer membrane is rendered in translucent blue and at one end surrounds an inner boundary membrane rendered in white that encloses two cristae rendered in red and in green; the outer membrane is ruptured at this end. At the other end is a single vesicular matrix compartment rendered in yellow.

Movie 4: Vesicular Swollen Mitochondrion: Model based upon a segmented EM Tomogram of a mitochondrion in a HeLa cell treated with Etoposide for 16 hours. Outer membrane is rendered in translucent blue and surrounds multiple vesicular matrix compartments of various sizes rendered in different colors. The magenta and yellow vesicular compartments appear to be swollen.

Movie 5: Mitochondrion model based upon a segmented EM Tomogram of a mitochondrion in a HeLa cell treated with Etoposide for 16 hours; this mitochondrion has not released cytochrome c, maintains a normal $\Delta\Psi$m, and appears normal in TEM thin sections. Outer membrane is rendered in translucent blue, inner boundary membrane rendered in opaque white with cristae rendered in different colors. Note that while some crista junctions appear normal others, particularly those of the magenta crista between the green and red cristae, are elongated around the periphery of the lamellar crista as predicted by the model in Supplementary Figure 3 and Movie 6.

Movie 6: Schematic model of the inner membrane of a normal orthodox mitochondrion transforming into vesicular matrix compartments; the outer membrane is not included. At the beginning two lamellar cristae are connected to the inner boundary membrane surrounding them through short tubular crista junctions, four in the upper crista and three in the lower crista. The inner boundary membrane is translucent light blue and the crista membrane is opaque yellow. The ends of the mitochondrion at the top and bottom are not modeled for simplification. As the movie progresses the crista junctions elongate around the periphery of the lamellar cristae eventually merging and fusing until the top and bottom halves of the lamellar cristae membranes become part of the vesicular matrix compartments that are modeled in opaque red, blue, and green at the end of the movie.

Movie 7: Normal Mitochondrion: Model based upon a segmented EM Tomogram of a control mitochondrion in a HeLa cell that has not been treated with Etoposide. Outer membrane is rendered in translucent blue, inner boundary membrane is rendered in opaque white, and cristae are rendered in various colors. Note relatively small and uniform discrete crista junctions connecting cristae to the inner boundary membrane.